Journal of Solid State Chemistry 183 (2010) 1464–1472

Contents lists available at ScienceDirect

Journal of Solid State Chemistry

journal homepage: www.elsevier.com/locate/jssc

Diversity of coordination modes in the polymers based on 3,3′,4,4′-biphenylcarboxylate ligand

Xiao-Di Du, Hong-Ping Xiao, Xin-Hui Zhou, Tao Wu, Xiao-Zeng You *

State Key Laboratory of Coordination Chemistry, Nanjing National Laboratory of Microstructures, School of Chemistry and Chemical Engineering, Nanjing University, Nanjing 210093, People's Republic of China

ARTICLE INFO

Article history:
Received 21 December 2009
Received in revised form
15 April 2010
Accepted 19 April 2010
Available online 24 April 2010

Keywords:
Coordination polymer
Crystal structure
Diversity of coordination modes
Multicarboxyl ligand

ABSTRACT

Four new compounds $[Ni_2(4,4'\text{-bpy})(3,4\text{-bptc})(H_2O)_4]_n$ (**1**), $[Ni(4,4'\text{-bpy})(3,4\text{-}H_2bptc)(H_2O)_3]_n$ (**2**), $[Mn_2(2,2'\text{-bpy})_4(3,4\text{-}H_2bptc)_2]$ (**3**) and $\{[Mn(1,10\text{-phen})_2(3,4\text{-}H_2bptc)]\cdot 4H_2O\}_n$ (**4**) (3,4-H_4bptc =3,3′,4,4′-biphenyltetracarboxylic acid, 4,4′-bpy=4,4′-bipyridine, 2,2′-bpy=2,2′-bipyridine, 1, 10-phen=1, 10-phenanthroline), have been prepared and structurally characterized. In all compounds, the derivative ligands of 3,4-H_4bptc (3,4-$bptc^{4-}$ and 3,4-H_2bptc^{2-}) exhibit different coordination modes and lead to the formation of various architectures. Compounds **1** and **2** display the three-dimensional (3D) framework: **1** shows a 3,4-connected topological network with $(8^3)(8^5\cdot 10)$ topology symbol based on the coordination bonds while in **2**, the hydrogen-bonding interactions are observed to connect the 1D linear chain generating a final 3D framework. **3** exhibits the 2D layer constructed from the hydrogen-bonding interactions between the dinuclear manganese units. Complex **4** shows the double layers motif through connecting the 1D zigzag chains with hydrogen-bonded rings. The thermal stability of **1**–**4** and magnetic property of **1** were also reported.

1. Introduction

Metal-organic coordination polymers based on the self-assembly of metal centers and multifunctional ligands have attracted much interest because of their intriguing variety of architectures, topologies, and potential applications as functional materials [1–12]. Among them, polycarboxylates have caught the long lasting research attention, due to their variety coordination modes and structural features, such as 1,2-benzenedicarboxylate, 1,4-benzenedicarboxylate, 1,3,5-benzenetricarboxylate, and 1,2,4,5-benzenetetracarboxylate, which all have been extensively employed in the construction of metal-organic polymers displaying variety structures and interesting properties [13–29]. So far, many efforts have been focused on the employment of flexible or the V-shaped multidentate organic bridging ligands [30–40], while the influence of the size of the rigid aromatic multidentate ligands on the formation of the ultimate framework have rarely been studied [41–58], especially for the paramagnetic transition metal coordination polymers [46–50,53–54,56–58].

3,3′,4,4′-biphenyltetracarboxylic acid (3,4-H_4bptc), which has eight oxygen atoms, is chosen to construct novel coordination polymers in view of its following characteristics: (1) it has four carboxyl groups that may be completely or partially deprotonated to form diversiform architectures and transmit magnetic interactions; (2) two phenyl rings can be rotated around the C–C bond, which results the 3,3′-carboxyl groups adopting the *trans*-conformation or *cis*-conformation; and (3) the oxygen atoms of the carboxyl groups can be regarded not only as hydrogen-bonding acceptors but also as hydrogen-bonding donors to form abundant hydrogen bonds, which are good for stabilizing and extending the solid-state structures. In order to understand the coordination chemistry of 3,4-H_4bptc with paramagnetic metal ions and prepare new materials with intriguing structure motif and excellent physical properties, we have recently engaged in the research of these kinds of metal-organic hybrid materials with this and related ligands.

In addition, the auxiliary ligands with pyridyl groups are usually introduced to the carboxylate systems for the construction of polymeric frameworks, which would combine the virtues of both functional groups as well as enhance the stability of the ultimate framework and obtain the target product more easily [59,60]. Thus, by introducing several N-containing auxiliary ligands, such as 4,4′-bipyridine (4,4′-bpy), 2,2′-bipyridine (2,2′-bpy) and 1,10-phenanthroline (1,10-phen), into the *M*-(3,4-H_4bptc) (*M*=paramagnetic transition metal) system, four coordination compounds $[Ni_2(4,4'\text{-bpy})(3,4\text{-bptc})(H_2O)_4]_n$ **(1)**, $[Ni(4,4'\text{-bpy})(3,4\text{-}H_2bptc)(H_2O)_3]_n$ **(2)**, $[Mn_2(2,2'\text{-bpy})_4(3,4\text{-}H_2bptc)_2]$ **(3)** and $\{[Mn(1,10\text{-phen})_2(3,4\text{-}H_2bptc)]\cdot 4H_2O\}_n$ **(4)** (3,4-H_4bptc=3,3′,4,4′-biphenyltetracarboxylic acid, 4,4′-bpy=4,4′-bipyridine, 2,2′-bpy=2,2′-bipyridine, 1,10-phen=1,10-phenanthroline) have been successfully prepared and characterized in this paper.

* Corresponding author. Fax: +86 25 83314502.
E-mail address: youxz@nju.edu.cn (X.-Z. You).

0022-4596/$ - see front matter © 2010 Elsevier Inc. All rights reserved.
doi:10.1016/j.jssc.2010.04.029

2. Experimental

2.1. Materials and general methods

The 3,3′,4,4′-biphenyltetracarboxylic acid (3,4-H_4bptc) was obtained through the hydrolysis of 4,4′-biphthalic anhydride that is purchased from Alfa Aesar. All other chemicals were of reagent grade and used as received. Elemental analyses for C, H, and N were performed on a Perkin-Elmer 240 °C analyzer. Infrared spectra were recorded on a Vector22 Bruker Spectrophotometer with KBr pellets in the 400 – 4000 cm^{-1} region. The powder XRD patterns were recorded on a Shimadzu XD-3A X-ray diffractometer. Thermogravimetric analyses (TGA) were collected on a Perkin-Elmer Pyris 1 TGA analyzer from room temperature to 700–800 °C with a heating rate of 20 °C/min under nitrogen. Magnetic susceptibility measurements of polycrystalline samples were measured over the temperature range 1.8 – 300 K with a Quantum Design MPMS-XL7 SQUID magnetometer.

2.2. Syntheses of complexes **1** – **4**

2.2.1. Syntheses of $[Ni_2(4,4'\text{-bpy})(3,4\text{-bptc})(H_2O)_4]_n$ **(1)** and $[Ni(4,4'\text{-bpy})(3,4\text{-}H_2bptc)\,(H_2O)_3]_n$ **(2)**.

A mixture of $Ni(NO_3)_2\cdot 6H_2O$ (1 mmol, 290.5 mg), 3,4-H_4bptc (0.35 mmol, 112 mg), 4,4′-bpy (0.38 mmol, 73.1 mg), H_2O (18 mL) was sealed in a 30 mL Teflon-lined bomb (pH = 4.5) and heated at 150 °C for 3 days. Then the reaction mixture was cooled to room temperature at a rate of 10 °C/h. Green block crystals of **1** and Green needle crystals of **2** suitable for X-ray diffraction analysis were isolated in 41% and 48% yield, respectively. Anal. Calcd for $C_{26}H_{22}N_2Ni_2O_{12}$ **(1)**: C, 46.48; H, 3.30; N, 4.17%. Found: C, 46.59; H, 3.48; N, 4.29%. IR (KBr)/cm^{-1} for **1**: 3416 (s), 1637 (s), 1617 (s), 1568 (s), 1541 (s), 1487 (m), 1404 (s), 1384 (s), 1074 (m), 992 (m), 817 (w), 779 (w), 709 (w), 620 (m), 476 (w). Anal. Calcd for $C_{26}H_{22}N_2NiO_{11}$**(2)**: C, 52.29; H, 3.71; N, 4.69%. Found: C, 52.19; H, 3.75; N, 4.81%. IR (KBr)/cm^{-1} for **2**: 3416 (s), 1701 (m), 1637(s), 1616 (s), 1540 (m), 1415 (m), 1384 (s), 1221 (w), 1139 (m), 1087 (m), 987 (m), 811 (m), 777 (m), 705 (m), 665 (m), 634 (m), 518 (w), 483 (w).

2.2.2. Syntheses of $[Mn_2(2,2'\text{-bpy})_4(3,4\text{-}H_2bptc)_2]$ **(3)**.

A mixture of $Mn(CH_3COO)_2\cdot 4H_2O$ (0.5 mmol, 130 mg), 3,4-H_4bptc (0.5 mmol, 165 mg), 2,2′-bpy (1 mmol, 156 mg), and H_2O (18 mL) was adjusted to pH 5 with a 0.5 M NaOH solution, then was sealed in a 30 mL Teflon-lined bomb and heated at 170 °C for 3 days. Then the reaction mixture was cooled to room temperature at a rate of 10 °C/h. Yellow block crystals of **3** suitable for X-ray diffraction analysis were isolated in 71% yield. Anal. Calcd for $C_{72}H_{48}Mn_2N_8O_{16}$: C, 62.17; H, 3.48; N, 8.06%. Found: C, 62.09; H, 3.43; N, 7.93%. IR (KBr)/cm^{-1}: 3443 (s), 1698 (m), 1608 (s), 1438 (sh), 1383 (s), 1288 (w), 1253 (w), 1149 (m), 993 (m), 859 (w), 826 (w), 806 (w), 765 (m), 736 (w), 705 (w), 670 (w), 624 (m), 538 (m).

2.2.3. Syntheses of $\{[Mn(1,10\text{-phen})_2(3,4\text{-}H_2bptc)]\cdot 4H_2O\}_n$ **(4)**.

A mixture of $Mn(CH_3COO)_2\cdot 4H_2O$ (0.5 mmol, 130 mg), 3,4-H_4bptc (0.5 mmol, 165 mg), 1,10-phen (0.55 mmol, 100 mg), MeOH (1 mL) and H_2O (18 mL) was adjusted to pH 4.3 with a 0.5 M NaOH solution, then was sealed in a 30 mL Teflon-lined bomb and heated at 160 °C for 3 days. Then the reaction mixture was cooled to room temperature at a rate of 10 °C/h. Yellow block crystals of **4** suitable for X-ray diffraction analysis were isolated in 78% yield. Anal. Calcd for $C_{40}H_{34}MnN_4O_{12}$: C, 58.76; H, 4.19; N, 6.85%. Found: C, 58.79; H, 4.39; N, 6.78%. IR (KBr)/cm^{-1}: 3473 (s), 3416 (s), 1697 (m), 1637 (s), 1618 (s), 1513 (m), 1422 (m), 1383 (s), 1299 (w), 1142 (m), 1100 (m), 992 (m), 846 (m), 805 (w), 780 (m), 765 (m), 726 (m), 619 (m), 482 (w).

2.3. X-ray crystallography

The crystal structures of complexes **1** – **4** were determined on a Siemens (Bruker) SMART CCD diffractometer using monochromated Mo–$K\alpha$ radiation ($\lambda = 0.71073$ Å) at room temperature. Cell parameters were retrieved using SMART software and refined using SAINT [13] on all observed reflections. Data were collected using a narrow-frame method with scan widths of 0.30° in ω and an exposure time of 10 s/frame. The highly redundant data sets were reduced using SAINT [61] and corrected for Lorentz and polarization effects. Absorption corrections were applied using SADABS [62] supplied by Bruker. Structures were solved by direct methods using the program SHELXL-97 [63]. The positions of the metal atoms and their first coordination spheres were located from direct-method E maps; other non-hydrogen atoms were found using alternating difference Fourier syntheses and least-squared refinement cycles and, during the final cycles, were refined anisotropically. Hydrogen atoms bonded to the oxygen atoms in **1**, O(10) in **2**, O(3) in **3**, and O(3) in **4** were found using difference Fourier syntheses method. All the other hydrogen atoms were placed in calculated position and refined as riding atoms with a uniform value of U_{iso}. Crystallographic details have been summarized in Table 1. Bond lengths and angles for the coordination environment are listed in Table 2. And the hydrogen-bonding geometry parameters are listed in Supplementary materials (Table S1).

3. Results and discussion

3.1. Synthesis and general characterization

Complexes **1**–**4** were obtained under the hydrothermal or solvothermal condition. All the compounds are stable in air. Compounds **1** and **2** were obtained from the same reaction and were separated manually. Combined with the results of X-ray structural analysis, a conclusion that the 3,4-$bptc^{4-}$ and 3,4-H_2bptc^{2-} anion are coexistent in the reaction system can be obtained.

The IR spectra of **1** – **4** all display the characteristic vibration peaks of carboxylate groups in the range 1630–1550 cm^{-1} for the asymmetric vibration and 1420–1300 cm^{-1} for the symmetric [64,65], although one major difference was observed between **1** and **2** – **4**. Compounds **2** – **4** show the characteristic bands of the carboxylic acid at around 1690 – 1730 cm^{-1} revealing that the deprotonation of the 3,4-H_4bptc is incomplete, while the absence of the corresponding peaks in **1**, indicates the complete deprotonation of the 3,4-H_4bptc ligand, which is consistent with the results of the X-ray analysis. The strong peaks around 1610 cm^{-1} can be attributed to the characteristic vibration peaks of the aromatic rings in the polycarboxyl and polypyridyl ligands. In addition, the less strong characterized bands for the polypyridyl coligands under 900 cm^{-1} (the out-of-plane motion of the C–H groups of the pyridyl rings) were also observed: 817 cm^{-1} in **1**, 811 cm^{-1} in **2**, 765 cm^{-1} in **3** and 846 cm^{-1}, 765 cm^{-1} in **4**. These bands in the regions of 860–800, 770–735 and 810–750 cm^{-1}may indicate that there are two, four, and three consecutive hydrogen atoms in the pyridyl rings [65], respectively. Based on it, the preliminary conclusion can be obtained: the polypyridyl coligands are not protonated but adopt the bidentate bridging coordination mode in **1** and **2**, and bidentate chelating coordination mode in **3** and **4**, which is consistent with the results of the X-ray analysis.

Table 1
Crystallographic data for complexes **1**–**4**.

	1	**2**	**3**	**4**
Formula	$C_{13}H_{11}NNiO_6$	$C_{26}H_{22}N_2NiO_{11}$	$C_{72}H_{48}Mn_2N_8O_{16}$	$C_{40}H_{34}MnN_4O_{12}$
F_w	335.94	597.17	1391.06	817.65
Crystal system	monoclinic	triclinic	monoclinic	monoclinic
Space group	*P*2(*1*)/*c*	*P*-1	P2(1)/*n*	P2(1)/*c*
a, Å	7.462(2)	10.0655(7)	15.019(4)	19.331(3)
b, Å	21.421(6)	11.3297(8)	10.491(3)	9.6655(16)
c, Å	9.2465(18)	12.4775(9)	22.026(4)	19.137(3)
α, deg.	90.00	94.6540(10)	90.00	90.00
β, deg.	122.601(14)	102.7290(10)	119.427(13)	90.830(3)
γ, deg.	90.00	114.1390(10)	90.00	90.00
V, Å^3	1245.1(5)	1242.92(15)	3022.8(13)	3575.3(10)
Z	4	2	2	4
D_{calcd}, g m^{-3}	1.792	1.596	1.528	1.519
T, K	298(2)	298(2)	298(2)	298(2)
μ, mm^{-1}	1.587	0.850	0.501	0.444
F(000)	688	616	1428	1692
Reflections collected	6156	6304	14833	17966
Unique reflections	2205	4349	5370	6632
GOF (F^2)	1.259	1.096	0.985	0.989
R_1[a],wR_2[b] ($I > 2\sigma(I)$)	0.0902, 0.2092	0.0335, 0.0897	0.0513, 0.0722	0.0584, 0.1664
R_1[a],wR_2[b](all data)	0.0975, 0.2131	0.0356, 0.0907	0.0874, 0.0790	0.0919, 0.1787

[a] $R_1 = \Sigma||F_o| - |F_c||/\Sigma|F_o|$.
[b] $wR_2 = [\Sigma w(F_o^2 - F_c^2)^2/\Sigma w(F_o^2)]^{1/2}$.

The observation of the peaks at ~630 cm^{-1}, which can be attributed to the M–N vibration [58], further indicate the polypyridyl coligands have take part in the coordination.

In the PXRD patterns for compounds **1**–**4** (Fig. S4, Supplementary materials), the diffraction peaks of both simulated and experimental patterns match well at the relevant positions, indicating the phase purities of **1**–**4**.

3.2. Structural description

3.2.1. $[Ni_2(4,4'\text{-bpy})(3,4\text{-bptc})(H_2O)_4]_n$ (1).

Single-crystal X-ray structural analysis showed that compound **1** crystallizes in the monoclinic space group $P2_1/c$. The asymmetric unit of **1** contains one Ni(II) ion, a half of 3,4-bptc^{4-}, a half of 4,4′-bpy and two coordinated water molecules. The nickel ion (Fig. 1) is six-coordinated by O(1) and O(3) from a 3,4-bptc^{4-} ligand in a chelating coordinated mode, O(4a) from another 3,4-bptc^{4-} ligand, N(1) from a 4,4′-bpy ligand and two water molecules O(5) and O(6). The coordination geometry around the nickel ion can be described as a slightly distorted octahedron with O(1), O(3), O(5), O(6) located in the equatorial plane and O(4), N(1) occupy the apical positions. The Ni–N bond length (2.044(7)Å) and Ni–O bond lengths (2.032(6)–2.146(7)Å) are comparable to those reported for Ni(II) complexes [66–68].

The 3,4-bptc^{4-} ligand in **1** (Scheme 1a) is full deprotonated and acts as a hexadentate ligand binding four Ni atoms: two carboxyl groups at the 3-positions of phenyl rings act as bidentate bridging groups and adopt a *syn–anti* coordination mode, which is seldom for the nickel complexes [69,70], while two carboxyl groups at the 4-positions of phenyl rings are monodentate coordinating groups in a *anti* mode. Two carboxyl groups in the same phenyl ring bind to a metal ions to form a seven-membered chelate rings. The pair of phenyl rings of the ligand is nearly coplanar with the dihedral angle 0° and distance between planes 0.0667 Å. Then the neighboring seven-membered chelate rings are further linked by the bidentate bridging carboxyl groups at the 3-positions of phenyl rings generating the infinite 1D Ni–COO chains along the *c*-axis. On the basis of the connection mode, an extended 2D netlike layer along the *bc*-plane is formed (Fig. 2). Furthermore, the 2D netlike layers are further linked by the rigid bidentate bridging 4,4′-bpy ligand to generate a 3D framework displaying a 3,4-connected topological network with $(8^3)(8^5\cdot 10)$ topological symbol (the long Schläfli symbol [71] is $(8_3.8.8_3)(8_2.8_2.8_2.8_2.8_2.*)$) by considering the 3,4-bptc^{4-} ligands as 4-connected nodes, nickel ions as 3-connected nodes and 4,4′-bpy ligands as linkers (Fig. 3).

3.2.2. $[Ni(4,4'\text{-bpy})(3,4\text{-}H_2bptc)(H_2O)_3]_n$ (2).

Single-crystal X-ray diffraction reveals that **2** is a 3D supramolecular framework based on hydrogen bonding interactions of the adjacent 1D chain $[Ni(4,4'\text{-bpy})(3,4\text{-}H_2bptc)(H_2O)_3]_n$. The asymmetric unit contains a Ni(II) ion, a 3,4-H_2bptc^{2-}, a 4,4′-bpy ligand and three coordinated water molecules (Fig. 4). The Ni (II) ion is six coordinated, connects one oxygen atom (O1) from one 3,4-H_2bptc^{2-} ligand, two nitrogen atoms (N1, N2a) from two bridging bidentate 4,4′-bpy ligands and three water molecules (O9, O10, O11) to display an octahedral geometry with O(1), O(9), O(10), and O(11) as the equatorial plane, and N1 and N(2a) on the axial sites. Each 4,4′-bpy ligand connects the adjacent two Ni centers in a bidentate bridging mode to form an extended $[Ni(4,4'\text{-bpy})]_n$ 1D linear chain with the angle of 179.53(6)° for N(2a)–Ni(1)–N(1). The Ni–N and Ni–O bond lengths fall in the range of 2.110(1)–2.120(1)Å and 2.052(1)–2.082(1)Å, respectively. The 3,4-H_2bptc^{2-} anion in **2** (Scheme 1b) is partially deprotonated with the 4,4′-carboxyl groups protonated and the 3,3′-carboxyl groups deprotonated. However, only one carboxyl group at the 3-positions of phenyl rings (O1) takes part in the coordination. Thus, the 3,4-H_2bptc^{2-} ligands bond to the Ni centers exhibiting as the monodentate ligand hanging on the 1D linear chain $[Ni(4,4'\text{-bpy})]_n$ to form an extended 1D $[Ni(4,4'\text{-bpy})(3,4\text{-}H_2bptc)(H_2O)_3]_n$ chain polymer along the *b*-axis (Fig. 5). Interestingly, there are abundant H-bond net including intramolecular and intermolecular hydrogen bonds: the existence of the intramolecular hydrogen bonds O(7)–H(7A)···O(6), O(9)–H(9B)···O(1), and O(9)–H(9B)···O(2)), with the average distance of donor and acceptor (d(D···A)) 2.664 Å, enhances the stability of the 1D $[Ni(4,4'\text{-bpy})(3,4\text{-}H_2bptc)(H_2O)_3]_n$ chain; the intermolecular hydrogen bonds O(10)–H(10A)···O(5d) connect the 1D extended chain to form the 2D supramolecular layer motif along the *bc*-plane (Fig. 6), which are further linked by the

Table 2
Bond lengths (Å) and angles (deg.) for the coordination environment of compounds **1**–**4**.

1			
Ni(1)–O(4a)	2.032(6)	Ni(1)–O(1)	2.035(6)
Ni(1)–O(5)	2.051(6)	Ni(1)–N(1)	2.044(7)
Ni(1)–O(3)	2.070(6)	Ni(1)–O(6)	2.146(7)
O(4)–Ni(1b)	2.032(6)	O(4a)–Ni(1)–O(1)	90.7(3)
O(4a)–Ni(1)–O(5)	96.4(2)	O(1)–Ni(1)–O(5)	84.1(3)
O(4a)–Ni(1)–N(1)	168.3(3)	O(1)–Ni(1)–N(1)	99.7(3)
O(5)–Ni(1)–N(1)	90.1(3)	O(4a)–Ni(1)–O(3)	85.1(2)
O(1)–Ni(1)–O(3)	87.4(3)	O(5)–Ni(1)–O(3)	171.3(3)
N(1)–Ni(1)–O(3)	89.9(3)	O(4a)–Ni(1)–O(6)	82.7(3)
O(1)–Ni(1)–O(6)	171.9(3)	O(5)–Ni(1)–O(6)	91.9(3)
N(1)–Ni(1)–O(6)	87.4(3)	O(3)–Ni(1)–O(6)	96.7(3)
2			
Ni(1)–O(11)	2.052 (2)	Ni(1)–O(1)	2.082(2)
Ni(1)–O(10)	2.082(2)	Ni(1)–O(9)	2.083(2)
Ni(1)–N(2a)	2.111(1)	Ni(1)–N(1)	2.121(2)
N(2)–Ni(1b)	2.111(2)	O(11)–Ni(1)–O(1)	90.03(6)
O(11)–Ni(1)–O(10)	87.73(7)	O(1)–Ni(1)–O(10)	175.86(6)
O(11)–Ni(1)–O(9)	176.25(6)	O(1)–Ni(1)–O(9)	93.51(5)
O(10)–Ni(1)–O(9)	88.66(6)	O(11)–Ni(1)–N(2a)	90.97(7)
O(1)–Ni(1)–N(2a)	92.48(6)	O(10)–Ni(1)–N(2a)	91.03(6)
O(9)–Ni(1)–N(2a)	90.10(6)	O(11)–Ni(1)–N(1)	89.14(6)
O(1)–Ni(1)–N(1)	87.05(6)	O(10)–Ni(1)–N(1)	89.43(6)
O(9)–Ni(1)–N(1)	89.82(6)	N(2a)–Ni(1)–N(1)	179.53(6)
3			
Mn(1)–O(7a)	2.059(2)	Mn(1)–O(1)	2.154(2)
Mn(1)–N(3)	2.253(2)	Mn(1)–N(1)	2.287(3)
Mn(1)–N(4)	2.293(3)	Mn(1)–N(2)	2.310(2)
O(7)–Mn(1a)	2.059(2)	O(7a)–Mn(1)–O(1)	91.54(8)
O(7a)–Mn(1)–N(3)	96.88(9)	O(1)–Mn(1)–N(3)	113.00(9)
O(7a)–Mn(1)–N(1)	98.43(9)	O(1)–Mn(1)–N(1)	154.58(9)
N(3)–Mn(1)–N(1)	89.06(9)	O(7a)–Mn(1)–N(4)	166.44(9)
O(1)–Mn(1)–N(4)	86.66(9)	N(3)–Mn(1)–N(4)	71.62(9)
N(1)–Mn(1)–N(4)	88.75(9)	O(7a)–Mn(1)–N(2)	99.93(9)
O(1)–Mn(1)–N(2)	84.47(9)	N(3)–Mn(1)–N(2)	155.39(9)
N(1)–Mn(1)–N(2)	70.84(9)	N(4)–Mn(1)–N(2)	93.27(9)
4			
Mn(1)–O(1)	2.097(3)	Mn(1)–O(5a)	2.162(3)
Mn(1)–N(1)	2.250(3)	Mn(1)–N(4)	2.254(3)
Mn(1)–N(2)	2.305(3)	Mn(1)–N(3)	2.305(3)
O(5)–Mn(1b)	2.162(3)	O(1)–Mn(1)–O(5a)	85.89(11)
O(1)–Mn(1)–N(1)	90.52(11)	O(5a)–Mn(1)–N(1)	97.36(12)
O(1)–Mn(1)–N(4)	108.41(11)	O(5a)–Mn(1)–N(4)	102.51(12)
N(1)–Mn(1)–N(4)	153.29(12)	O(1)–Mn(1)–N(2)	162.87(11)
O(5a)–Mn(1)–N(2)	92.86(11)	N(1)–Mn(1)–N(2)	72.67(12)
N(4)–Mn(1)–N(2)	88.56(12)	O(1)–Mn(1)–N(3)	96.36(11)
O(5a)–Mn(1)–N(3)	174.93(12)	N(1)–Mn(1)–N(3)	87.18(12)
N(4)–Mn(1)–N(3)	72.47(12)	N(2)–Mn(1)–N(3)	86.33(11)

Symmetry codes: **[1]**: (a) x, $-y+1/2$, $z+1/2$; (b) x, $-y+1/2$, $z-1/2$.**[2]**: (a) x, $y-1$, z; (b) x, $y+1$, z.**[3]**: (a) $x-1/2$, $-y+3/2$, $z+1/2$.**[4]**: (a) x, $-y+1/2$, $z-1/2$; (b) x, $-y+1/2$, $z+1/2$.

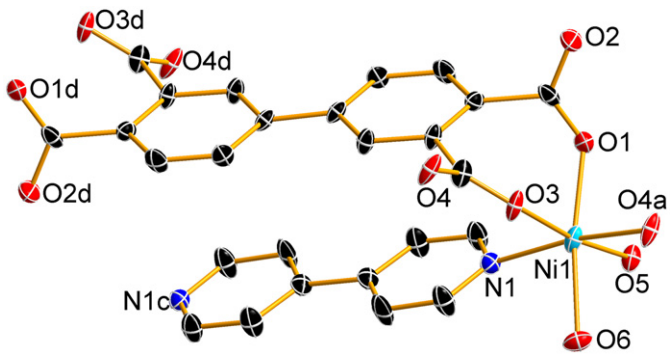

Fig. 1. View of the coordination environment of Ni(II) ion in **1**. All H atoms are omitted for clarity. Symmetry codes: (a) x, $-y+1/2$, $z+1/2$; (c) $-x+1$, $-y$, $-z+1$; (d) $-x+2$, $-y$, $-z+1$.

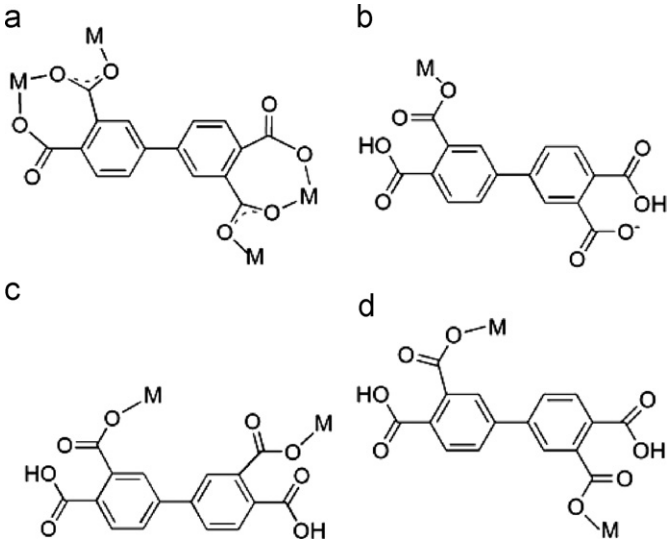

Scheme 1. Coordination modes of the 3,4-bptc^{4-} and 3,4-H_2bptc^{2-} ligands in **1**–**4**.

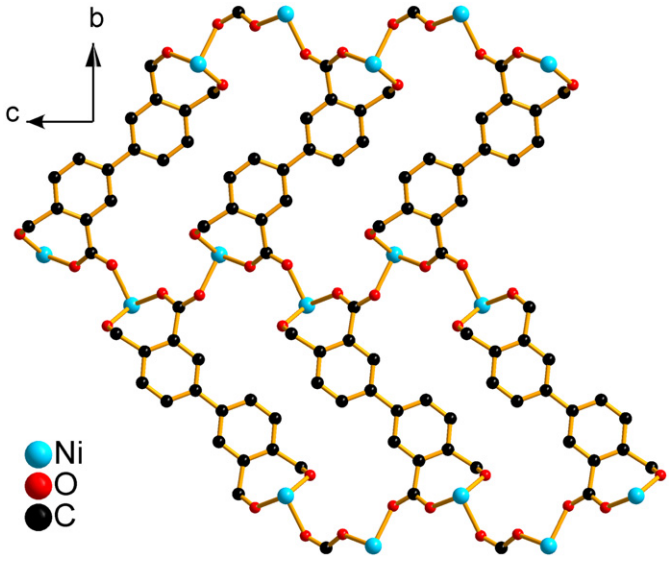

Fig. 2. The 2D layer in compound **1** based on the Ni (II) ions and 3,4-bptc^{4-} ligands along the *bc*-plane.

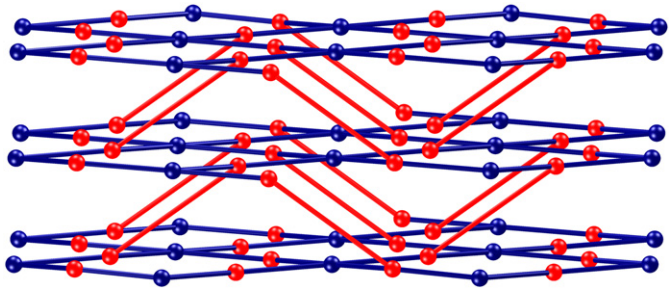

Fig. 3. Topological representation of the 3D framework in complex **1** showing the 3,4-connected topological network with $(8^3)(8^5\cdot 10)$ topological symbol.

O(11)–H(11A)···O(8c), O(11)–H(11B)···O(1e), O(10)–H(10B)···O(7c), O(9)–H(9A)···O(3b), O(4)–H(4A)···O(5a) intermolecular hydrogen bonds, with the average d(D···A) of 2.743 Å, to form a

3D supermolecular architecture (Table S1 and Fig. S1, Supplementary materials).

3.2.3. $[Mn_2(2,2'\text{-bpy})_4(3,4\text{-}H_2bptc)_2]$ (3).

The asymmetric unit of **3** contains a Mn (II) ion, a 3,4-H_2bptc^{2-} ligand and two 2,2′-bpy ligands (Fig. 7). The 3,4-H_2bptc^{2-} ligand adopt a bidentate mode (Scheme 1c): the 4,4′-carboxyl groups are both protonated and do not take part in the coordination, two 3,3′-carboxyl groups display a *cis*-conformation and adopt two monodentate bridging mode, connecting two Mn (II) ions to form a dinuclear Mn (II) unit with the Mn (1)···Mn (1a) distance of 8.074(1) Å. The dihedral angle between the pair of phenyl rings of the 3,4-H_2bptc^{2-} ligand is 13.95(8)°. Each Mn (II) center has a distorted octahedron coordination environment and is six-coordinated by N(1), N(2), N(3) and N(4) from two chelated 2,2′-bpy ligand, O(1) and O(7a) from two *cis*-3,4-H_2bptc^{2-} ligands. Furthermore, the 4,4′-COOH groups are bonded to each other by hydrogen boding interaction (O(6)–H(6)···O(3a) and O(6)–H(6)···O(4a)). As shown in Fig. 8, each dimeric Mn_2 unit joined to four dimeric Mn_2 units in its neighborhood forming a final 2D layer along the *ab* plane (Table S1, Supplementary materials).

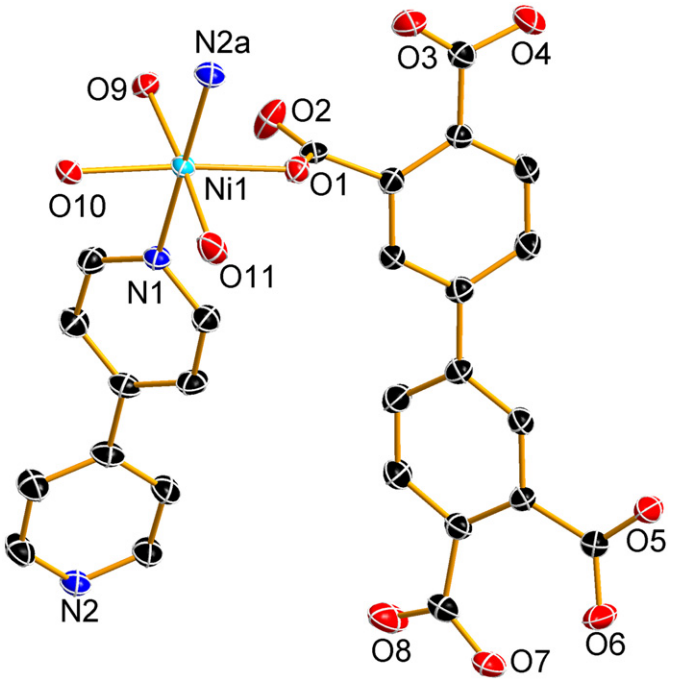

Fig. 4. View of the asymmetric unit of **2** with the thermal ellipsoids drawn at the 50% probability level. All H atoms are omitted for clarity. Symmetry code: (a) $x, y-1, z$.

3.2.4. $\{[Mn(1,10\text{-phen})_2(3,4\text{-}H_2bptc)]\cdot 4H_2O\}_n$ (4).

The asymmetric unit of 4 contains a Mn (II) ion, a 3,4-H_2bptc^{2-} ligand, two 1,10-phen ligands and four lattice water molecules (Fig. 9). The coordination mode of the 3,4-H_2bptc^{2-} ligand and the chelate ligand around the metal center are both similar to that in **3**. The major difference is that the two 3,3′-carboxyl groups in **3** display the *cis*-conformation while the *trans*-conformation in 4 (Scheme 1d), which results the great differences between the two structures: compound **4** displays an 1D zigzag chain $[Mn(1,10\text{-phen})_2(3,4\text{-}H_2bptc)]_n$ along *c*-axis (Fig. 10) while **3** exhibits a dinuclear unit. Upon this comparison, we can find that the size of the auxiliary ligands plays an important part of the formation and structures of the resulting compounds. Interestingly, the crystal water molecules in **4** are linked by the hydrogen-bonding interactions O(9)–H(9A)···O(13), O(10)–H(10B)···O(13), O(10)–H(10A)···O(11), and O(9)–H(9B)···O(11c) to form circlic octameric water clusters with the average d(D···A) of 2.709 Å, similar water circles have also been observed in some metal organic frameworks [72,73]. Then the water clusters link the 1D zigzag chains $[Mn(1,10\text{-phen})_2(3,4\text{-}H_2bptc)]_n$ along *b*-axis through the hydrogen bonds O(9)–H(9A)···O(2b), O(11)–H(11A)···O(2d), O(13)–H(13B)···O(1b), O(13)–H(13B)···O(5d), and O(3)–H(3A)···O(9a) with the average d(D···A) of 2.92 Å, to form the double-layers along the *bc*-plane (Table S1 and Fig. S2–3, Supplementary materials).

3.3. Diversity of coordination modes for 3,4-bptc^{4-} and 3,4-H_2bptc^{2-} in 1–4.

In compounds **1–4**, two polycarboxyl anions 3,4-bptc^{4-} and 3,4-H_2bptc^{2-} are observed. They are the more common forms of the deprotonated anions for 3,4-H_4bptc that have ever been observed, including 3,4-bptc^{4-} [43,45,47,49,50,54–58], 3,4-H_2bptc^{2-} [42–44,46–48,51–54], and 3,4-H_3bptc^{-} [49]. In compound **1**, the 3,4-bptc^{4-} ligand displays a new coordination mode in the 3,4-bptc^{4-} based system. For the 3,4-bptc^{4-}, it often acts as a quadridentate or hexadentate ligand, with all the carboxylic groups adopting the monodentate mode [49,54,57] or two carboxylic groups adopting the bidentate bridging mode while the other exhibiting the bidentate chelating mode [45,49,54]. However, the combination of bidentate bridging mode with monodentate mode is still rarely observed [43] and is different from that in **1**. In **2–4**, the common form for 3,4-H_2bptc^{2-} ligand with the 4,4′-carboxyl groups protonated and the 3,3′-carboxyl groups deprotonated [43,46–48,51–54] are observed. However, the coordination mode are different from the most common adoption in the references, which utilize one

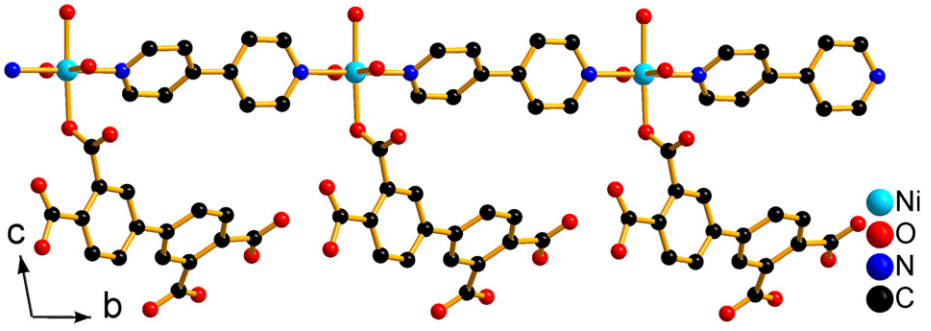

Fig. 5. The 1D chain structure in **2**. All H atoms are omitted for clarity.

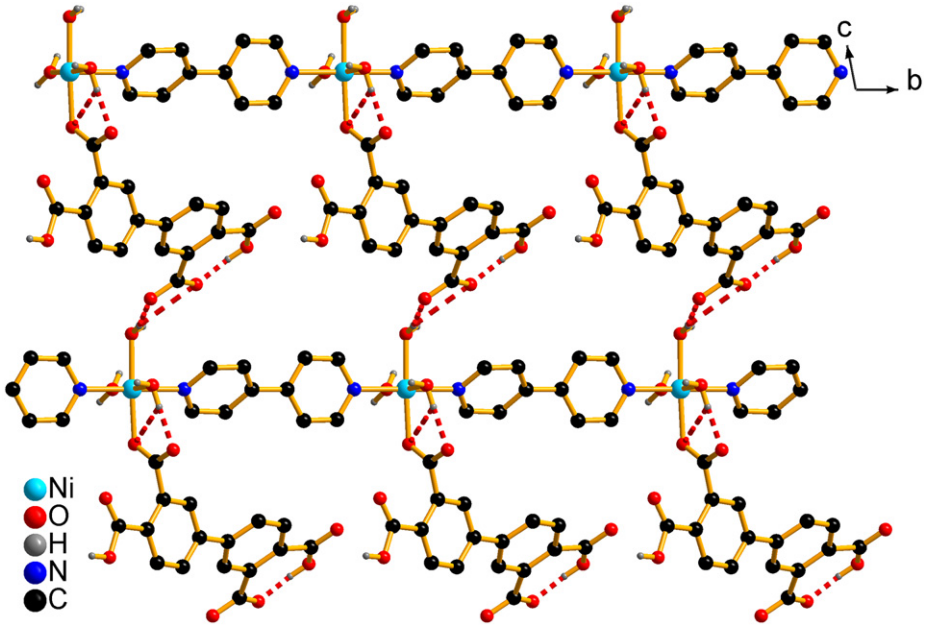

Fig. 6. The 2D layer motif formed by hydrogen bonding interaction in complex **2** along the *bc*-plane. The dashed lines represent the hydrogen bonding interaction.

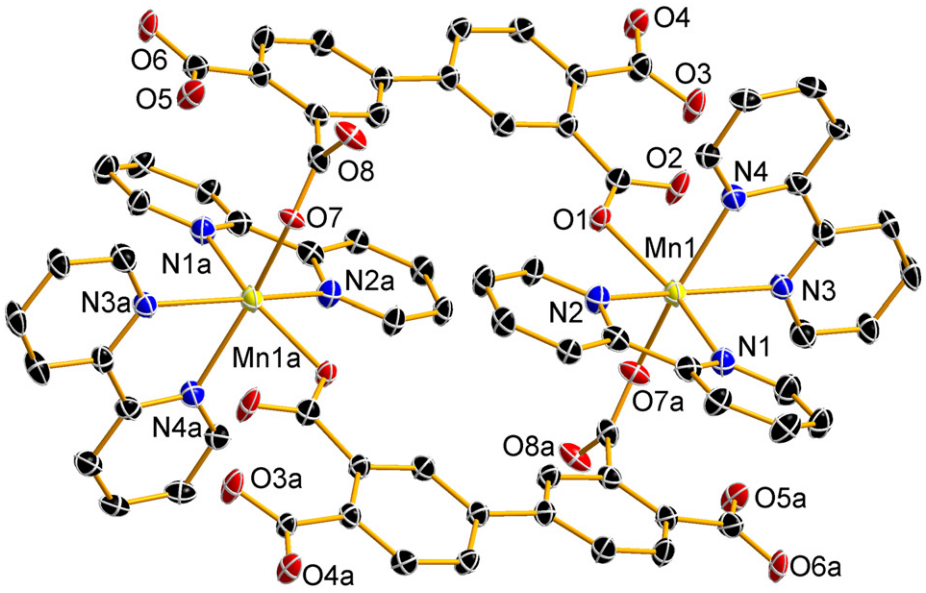

Fig. 7. The dinuclear unit of complex **3**. All H atoms are omitted for clarity. Symmetry code: (a) $-x+1$, $-y+1$, $-z+2$.

carboxyl group as the bidentate bridge and the other as the bidentate chelate [43,46–48,51], though that of **4** had been observed in Ref. [47]. And the coordination modes in **2** and **3** have not seen before in this system.

3.4. Magnetic properties

The temperature-dependent magnetic susceptibility data of complex **1** have been measured for polycrystalline samples in the temperature range 1.8–300 K under a 2000 Oe applied magnetic field, as shown in Fig. 11.

In compound **1**, the nickel (II) ions are connected by the bridging carboxylate groups of 3,4-bptc^{4-} ligands in a *syn–anti* mode displaying the 1D Ni–COO chains with the distances of the close and alternate Ni(II) ions 5.134(2) Å and 9.247(2) Å, respectively. The shortest distances of the inter-chains linked by 3,4-bptc^{4-} and 4,4′-bpy ligands are 11.528(3) Å and 11.06(2) Å, respectively, which are too long for significant magnetic interactions. So the magnetic interactions in **1** are mainly transmitted by the 1D Ni−COO chains. As shown in Fig. 11, at 300 K, the $\chi_M T$ value of **1** is 3.71 emu K mol^{-1}, which is slight higher than the spin-only value for three uncorrelated $S=1$ Ni(II) centers (3.0 emu K mol^{-1}). This difference might be caused by the spin–orbit coupling characteristic for nickel (II) complexes with an $^3A_{2g}$ ground state resulting in an increasing g factor [74,75]. Upon cooling to 18 K, the $\chi_M T$ value increases slowly and reaches the maximum of 3.75 emu K mol^{-1}, then, it decreases rapidly to

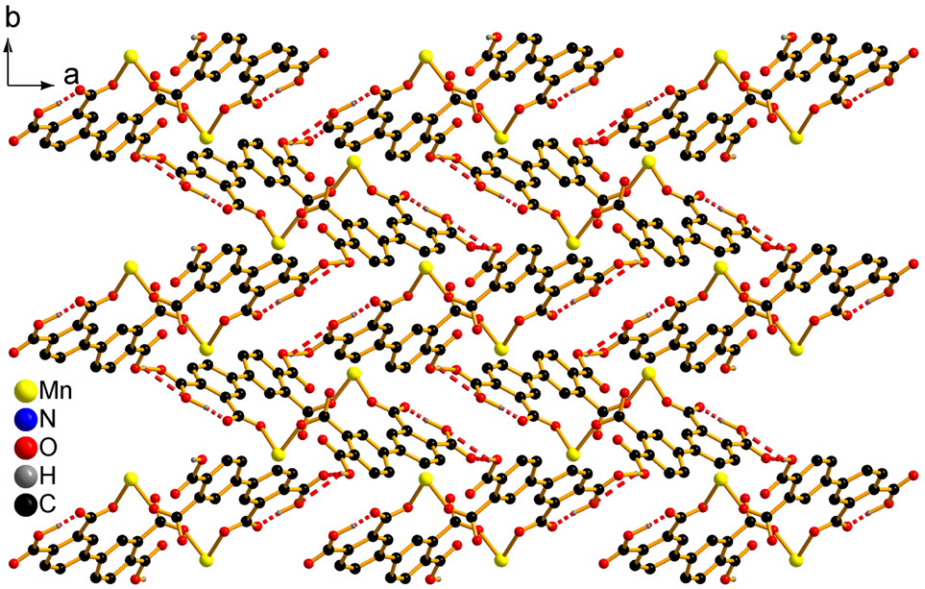

Fig. 8. The 2D layer formed by hydrogen bonding interaction in complex **3** along the *ab*-plane. The dashed lines represent the hydrogen bonding interaction.

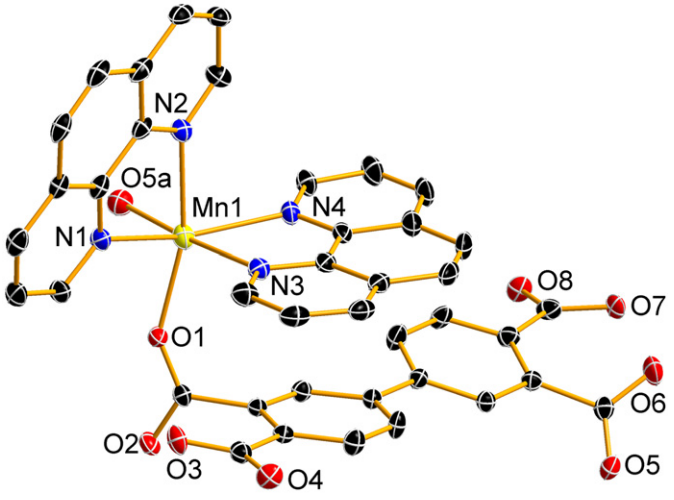

Fig. 9. The asymmetric unit of **4** with the thermal ellipsoids drawn at the 50% probability level. All H atoms are omitted for clarity. Symmetry code: (a) x, $-y+1/2$, $z-1/2$.

1.96 emu K mol^{-1} at 1.8 K, indicating the ferromagnetic coupling between the neighboring nickel ions in the 1D Ni–COO chains of **1** and antiferromagnetic interaction within the inter-chains at low temperature. The experimental data was modeled in the range from 300 to 1.8 K using the Ginsberg's method [18] deduced from the Hamiltonian $H=-2J[S_1S_2+S_2S_3]$ for linear Ni (II) trimer by eliminating the coupling between the two terminal Ni (II) ions in the trimers. The formula of $\chi_M T$ vs. T is as follows:

$$\chi_M T = Ng^2\beta^2(F(J))T/(kT-J'F(J))$$

where

$$F(J) = 28+10\exp(-J/kT)+2\exp(-2J/kT)+2\exp(-3J/kT) +10\exp(-3J/kT)+2\exp(-5J/kT)/7+5\exp(-J/kT) +3\exp(-2J/kT)+3\exp(-3J/kT)+5\exp(-3J/kT) +\exp(-4J/kT)+3\exp(-5J/kT)$$

In the formula, J is the exchange interaction between adjacent nickel (II) ions, S_i is the spin operate for each $S=1$ Ni(II), J' represents the interactions between the Ni–COO chains. A satisfactory fit was obtained with the parameters $g=2.22$, $J=2.48\,\mathrm{cm}^{-1}$, and $J'=-0.83$, confirming the ferromagnetic interactions in **1**, which is in agreement with the results [69] that the syn–anti carboxylate complexes are often ferromagnetically coupled for copper (II) and nickel (II) complexes although the number of nickel (II) complexes in the literature is very poor [69,70].

3.5. Thermal analysis

Thermogravimetric analyses (TGA) have been measured for complexes **1**–**4**. As shown in Fig. 12, complex **1** displays two weight loss stages, giving a total loss of 79.58% in the range 23–750 °C, which approximately agrees with the calculated value of 77.76%. The weight loss of 11.64% (calcd 10.73%) of the first step (23–248 °C) corresponds to the release of the coordinated water molecules. The second step occurred between 248 and 473 °C corresponds to the oxidation of the 4,4′-bpy and the 3,4-bptc^{4-} ligands. Complex **2** shows a continuous weight loss of 86.04% (calcd 87.48%) in the 23 – 565 °C. Complex **3** also displays two main steps of weight losses and begins to collapse at 409 °C with the total weight loss of 87.94% (calcd 87.50%). For complex **4**, a weight loss of 8.30% (calcd 8.81%) in the range 23–76 °C corresponds to the release of the lattice water molecules, then the decomposition of other residual components started beyond 226 °C.

4. Conclusion

In summary, four coordination compounds based on the 3,3′,4,4′-biphenyltetracarboxylic acid (3,4-H_4bptc) ligand and paramagnetic transition metal ions (nickel (II) or manganese (II)) have been successfully synthesized and four coordination modes of the 3,4-H_4bptc ligand, with three new for the 3,4-H_4bptc system (Scheme 1a, b and c) are observed in these complexes resulting the diversified architectures from 0D dinuclear unit to 3D network, which suggest that the different coordination modes of the 3,4-H_4bptc ligand may be affected by the experimental conditions, such as the metal centers, pH values, as well as size of

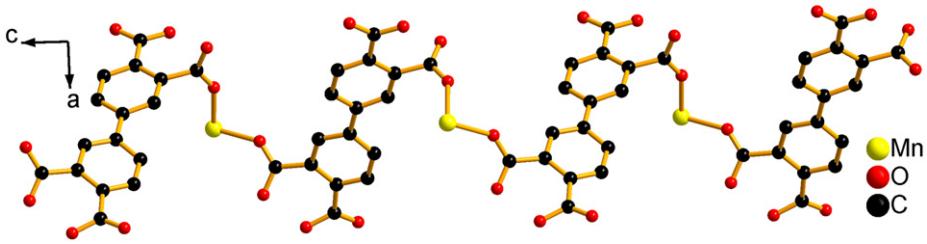

Fig. 10. View of the 1D zigzag chain of **4** along the *c*-axis.

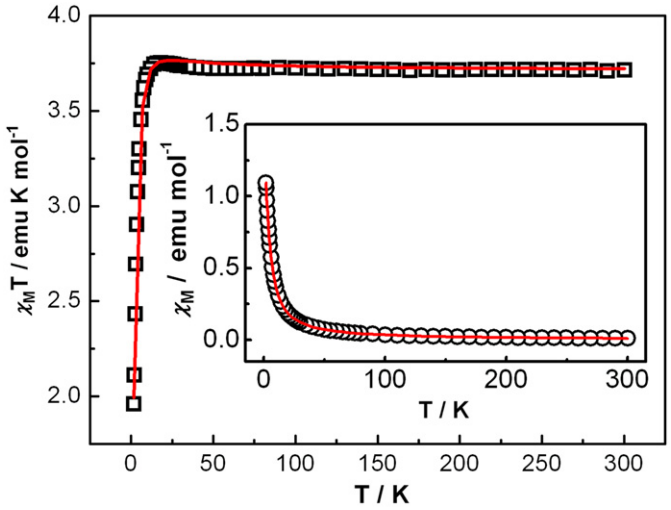

Fig. 11. Temperature dependences of the $\chi_M T$ (□) and χ_M (○) curves for complex **1**.

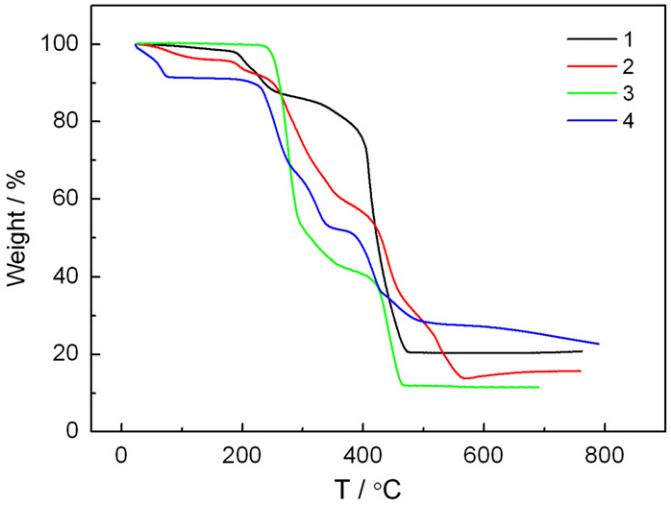

Fig. 12. Thermogravimetric curves for **1**–**4**.

the auxiliary ligands. The existence of abundant hydrogen-bonding interactions in these systems further enhances the stability and extends the corresponding architectures to form high dimensional framework.

Acknowledgments

This work was supported by the National Basic Research Program of China (2006CB806104 and 2007CB925100), and the National Natural Science Foundation of China (20721002), and the funding from Academician Workstation in Changzhou Trina Solar Energy Co., Ltd., Jiangsu Province.

Appendix A. Supplementary materials

The PXRD patterns, FTIR figures, hydrogen-bonding geometry parameters and the views of the hydrogen-bonding interactions for **1**–**4**. CCDC reference numbers 748900, 748901, 748903, and 748904.

CCDC 748900, 748901, 748903, and 748904 contain the supplementary crystallographic data for **1**, **2**, **3**, and **4**. These data can be obtained free of charge via 〈http://www.ccdc.cam.ac.uk/conts/retrieving.html〉, or from the Cambridge Crystallographic Data Centre, 12 Union Road, Cambridge CB2 1EZ, UK; fax: (+44) 1223 336 033; or e-mail: deposit@ccdc.cam.ac.uk.

Appendix B. Supplementary data

The online version of this article contains additional supplementary data. Please visit doi:10.1016/j.jssc.2010.04.029

References

[1] S.R. Batten, R. Robson, Angew. Chem. Int. Ed. 37 (1998) 1460.
[2] S.R. Batten, CrystEngComm 3 (2001) 67.
[3] B.F. Hoskins, R. Robson, J. Am. Chem. Soc. 112 (1990) 1546.
[4] M. Fujita, Y.J. Kwon, S. Washizu, K. Ogura, J. Am. Chem. Soc. 116 (1994) 1151.
[5] O.M. Yaghi, H. Li, C. Davis, D. Richardson, T.L. Groy, Acc. Chem. Res. 31 (1998) 474.
[6] S.Q. Ma, X.S. Wang, D.Q. Yuan, H.C. Zhou, Angew. Chem. Int. Ed. 47 (2008) 4130.
[7] L. Carlucci, G. Ciani, D.M. Proserpio, Coord. Chem. Rev. 246 (2003) 247.
[8] A.N. Khlobystov, A.J. Blake, N.R. Champness, D.A. Lemenovskii, A.G. Majouga, N.V. Zyk, M. Schröer, Coord. Chem. Rev. 222 (2001) 155.
[9] H. Guo, G. Zhu, I.J. Hewitt, S. Qiu, J. Am. Chem. Soc. 131 (2009) 1646.
[10] R.E. Morris, P.S. Wheatley, Angew. Chem. Int. Ed. 47 (2008) 4966.
[11] A. Comotti, S. Bracco, G. Distefano, P. Sozzani, Chem. Commun. (2009) 284.
[12] M. Eddaoudi, J. Kim, N. Rosi, D. Vodak, J. Wachter, M. O'Keeffe, O.M. Yaghi, Science 295 (2002) 469.
[13] F.A. Cotton, C.A. Murillo, X. Wang, R. Yu, Inorg. Chem. 43 (2004) 8394.
[14] J. Yang, G.D. Li, J.J. Cao, Q. Yue, G.H. Li, J.S. Chen, Chem. Eur. J. 13 (2007) 3248.
[15] J. He, Y. Zhang, J. Yu, Q.R. Xu, Mater. Res. Bull. 41 (2006) 925.
[16] X. Wang, L. Liu, A.J. Jacobson, Angew. Chem. Int. Ed. 45 (2006) 6499.
[17] C. Daiguebonne, N. Kerbellec, K. Bernot, Y. Gerault, A. Deluzet, O. Guillou, Inorg. Chem. 45 (2006) 5399.
[18] B. Moulton, H. Abourahma, M.W. Bradner, J. Lu, G.J. McManus, M.J. Zaworotko, Chem. Commun. (2003) 1342.
[19] C. Ma, C. Chen, Q. Liu, D. Liao, L. Li, L. Sun, New J. Chem. 27 (2003) 890.
[20] Y. Liu, J.F. Eubank, A.J. Cairns, J. Eckert, V.C. Kravtsov, R. Luebke, M. Eddaoudi, Angew. Chem. Int. Ed. 46 (2007) 3278.
[21] F. Luo, Y.X. Che, J.M. Zheng, Inorg. Chem. Commun. 9 (2006) 848.
[22] J. He, Y. Zhang, Q. Pan, J. Yu, H. Ding, R. Xu, Microporous Mesoporous Mater. 90 (2006) 145.
[23] F.A.A. Paz, J. Klinowski, Inorg. Chem. 43 (2004) 3948.
[24] X. Zhao, B. Xiao, A.J. Fletcher, K.M. Thomas, D. Bradshaw, M.J. Rosseinsky, Science 306 (2004) 1012.
[25] F.A. Cotton, L.M. Daniels, C. Lin, C.A. Murillo, Chem. Commun. (1999) 841.
[26] D. Sun, R. Cao, Y. Liang, Q. Shi, M. Hong, Dalton Trans. (2002) 1847.
[27] L.P. Sun, S.Y. Niu, J. Jin, G.D. Yang, L. Ye, Eur. J. Inorg. Chem. (2006) 5230.
[28] X.Y. Wang, S.C. Sevov, Inorg. Chem. 47 (2008) 1037.

[29] M.A. Braverman, R.L. LaDuca, CrystEngComm 10 (2008) 117.
[30] J. Zhang, Z.J. Li, J.K. Cheng, Y. Kang, Y.Y. Qin, Y.G. Yao, New J. Chem. 29 (2005) 421.
[31] P.X. Yin, Z.J. Li, X.Y. Cao, Y.Y. Qin, Y.G. Yao, Acta Cryst. E 63 (2007) m2258.
[32] D.R. Xiao, E.B. Wang, H.Y. An, Y.G. Li, Z.M. Su, C.Y. Sun, Chem. Eur. J. 12 (2006) 6528.
[33] D.R. Xiao, E.B. Wang, H.Y. An, Y.G. Li, L. Xu, Cryst. Growth Des. 7 (2007) 506.
[34] S.L. Li, Y.Q. Lan, J.F. Ma, J. Yang, G.H. Wei, L.P. Zhang, Z.M. Su, Cryst. Growth Des. 8 (2008) 675.
[35] J. Zhang, Z.J. Li, Y. Kang, J.K. Cheng, Y.G. Yao, Inorg. Chem. 43 (2004) 8085.
[36] D.R. Xiao, Y.G. Li, E.B. Wang, L.L. Fan, H.Y. An, Z.M. Su, L. Xu, Inorg. Chem. 46 (2007) 4158.
[37] X.L. Chen, B. Zhang, H.M. Hu, F. Fu, X.L. Wu, T. Qin, M.L. Yang, G.L. Xue, J.W. Wang, Cryst. Growth Des. 8 (2008) 3706.
[38] S.Q. Zang, Y. Su, Y.Z. Li, Z.P. Ni, Q.J. Meng, Inorg. Chem. 45 (2006) 174.
[39] Y. Su, S.Q. Zang, Y.Z. Li, H.Z. Zhu, Q.J. Meng, Cryst. Growth Des. 7 (2007) 1277.
[40] X.Y. Duan, Y.Z. Li, Y. Su, S.Q. Zang, C.J. Zhu, Q.J. Meng, CrystEngComm 9 (2007) 758.
[41] S.Q. Zang, Y. Su, Y.Z. Li, Z.P. Ni, H.Z. Zhu, Q.J. Meng, Inorg. Chem. 45 (2006) 3855.
[42] X.L. Wang, C. Qin, E.B. Wang, L. Xu, Eur. J. Inorg. Chem. (2005) 3418.
[43] J.J. Wang, L. Gou, H.M. Hu, Z.X. Han, D.S. Li, G.L. Xue, M.L. Yang, Q.Z. Shi, Cryst. Growth Des. 7 (2007) 1514.
[44] X.L. Wang, C. Qin, E.B. Wang, Cryst. Growth Des. 6 (2006) 439.
[45] J.J. Wang, M.L. Yang, H.M. Hu, G.L. Xue, D.S. Li, Q.Z. Shi, Z. Anorg. Allg. Chem. 633 (2007) 341.
[46] C. Qin, X.L. Wang, E.B. Wang, Acta Cryst. E 63 (2007) m3073.
[47] G.P. Yang, Y.Y. Wang, L.F. Ma, J.Q. Liu, Y.P. Wu, W.P. Wu, Q.Z. Shi, Eur. J. Inorg. Chem. (2007) 3892.
[48] X.R. Hao, Z.M. Su, Y.H. Zhao, K.Z. Shao, Y. Wang, Acta Cryst. E 61 (2005) m2477.
[49] S.R. Zhu, H.Z. Zhang, M.S. Shao, Y.M. Zhao, M. X. Li, Transition Met. Chem. 33 (2008) 669.
[50] L.X. Sun, Y. Qi, Y.X. Che, S.R. Batten, J.M. Zheng, Cryst. Growth Des. 9 (2009) 2995.
[51] X.R. Hao, Z.M. Su, Y.H. Zhao, K.Z. Shao, Y. Wang, Acta Cryst. C 61 (2005) m469.
[52] J. Kang, C.C. Huang, Z.Q. Jiang, S. Huang, S.L. Huang, Acta Cryst. E 65 (2009) m452.
[53] J. Kang, C.C. Huang, L.S. Zhai, X.H. Qin, Z.Q. Liu, Acta Cryst. E 65 (2009) m380.
[54] G.X. Liu, K. Zhu, H. Chen, R.Y. Huang, X.M. Ren, Z. Anorg. Allg. Chem. 635 (2009) 156.
[55] D.F. Weng, X.J. Zheng, L.C. Li, W.W. Yang, L.P. Jin, Dalton Trans. (2007) 4822.
[56] D. Zhou, M. Shao, X. He, Y.M. Zhao, S.R. Zhua, Acta Cryst. E 65 (2009) m562.
[57] S.J. Deng, N. Zhang, W.M. Xiao, C. Chen, Inorg. Chem. Commun. 12 (2009) 157.
[58] G.P. Yang, Y.Y. Wang, H. Wang, C.J. Wang, G.L. Wen, Q.Z. Shi, S.M. Peng, J. Mol. Struct. 888 (2008) 366.
[59] H. Chun, J. Am. Chem. Soc. 130 (2007) 800.
[60] R. Kitaura, K. Seki, G. Akiyamam, S. Kitagawa, Angew. Chem. Int. Ed. 42 (2003) 428.
[61] SAINT-Plus, version 6.02; Bruker Analytical X-ray System: Madison, WI, 1999.
[62] G. M. Sheldrick, SADABS, An empirical absorption correction program; Bruker Analytical X-ray Systems: Madison, WI, 1996.
[63] G. M. Sheldrick, SHELXTL-97; Universität of Göttingen: Göttingen, Germany, 1997.
[64] L.J. Bellamy, The Infrared Spectra of Complex Molecules, John Wiley & Sons, New York, 1958.
[65] D.H. Williams, I. Fleming, Spectroscopic Methods in Organic Chemistry, McGraw-Hill, Cambridge, 1995.
[66] X.L. Wang, C. Qin, E.B. Wang, Y.G. Li, Z.M. Su, L. Xu, L. Carlucci, Angew. Chem. Int. Ed. 44 (2005) 5824.
[67] T.M. Cocker, R.E. Bachman, Chem. Commun. (1999) 875.
[68] H.A. Miller, N. Liang, S. Parsons, A. Parkin, P.A. Tasker, D.J. White, J. Chem. Soc., Dalton Trans. (2000) 3773.
[69] P.S. Mukherjee, S. Konar, E. Zangrando, T. Mallah, J. Ribas, N.R. Chaudhuri, Inorg. Chem. 42 (2003) 2695.
[70] X.H. Zhou, X.D. Du, G.N. Li, J.L. Zuo, X.Z. You, Cryst. Growth Des. 9 (2009) 4487.
[71] D. Braga, F. Grepioni, Making Crystals by Design, WILEY-VCH Verlag GmbH & Co, KGaA, Weinheim, 2007.
[72] J.L. Atwood, L.J. Barbour, T.J. Ness, C.L. Raston, P.L. Raston, J. Am. Chem. Soc. 123 (2001) 7192.
[73] P. Yang, X. Chen, S. Ren, S.L. Ma, Struct. Chem. 19 (2008) 291.
[74] A. Earnshaw, Introduction to Magnetochemistry, Academic Press, London, 1968.
[75] R.L. Carlin, Magnetochemistry, Springer, Berlin, 1986.